Magn Reson Mater Phy (2007) 20:27–37
DOI 10.1007/s10334-006-0066-7

RESEARCH ARTICLE

An iron-based T_1 contrast agent made of iron-phosphate complexes: In vitro and in vivo studies

Elisenda Rodríguez · Rui V. Simoes · Anna Roig · Elies Molins · Nataliya Nedelko · Anna Ślawska-Waniewska · Silvio Aime · Carles Arús · Miquel E. Cabañas · Coral Sanfeliu · Sebastián Cerdán · Maria Luisa García-Martín

Received: 6 April 2006 / Accepted: 12 December 2006 / Published online: 1 February 2007

Abstract A new iron-based T_1 contrast agent consisting of a complex of iron ions coordinated to phosphate and amine ligands ($Fe_{(phos)}$ in short) has been characterized by spectroscopic and magnetic measurements. NMR relaxation studies showed r_1 values to be dependent on the phosphate salt concentration, K_2HPO_4, present in the medium. r_1 reaches a maximum value of 2.5 $mM^{-1}\,s^{-1}$ for measurements carried out at 7 T and 298 K. ^{31}P MRS, Mössbauer spectroscopy and magnetic measurements of $Fe_{(phos)}$ solutions suggest paramagnetic Fe^{3+} ions present in the studied iron–phosphate complex. In vitro and in vivo toxicity experiments with C6 cells and CD1 mice, respectively, demonstrated lack of toxicity for $Fe_{(phos)}$ at the highest dose tested in the MRI experiments (12 mM iron for C6 cells and 0.32 mmol iron/kg for mice). Finally, T_1 weighted images of brain tumours in mice have shown positive contrast enhancement of $Fe_{(phos)}$ for tumour afflicted regions in the brain.

Keywords Magnetic resonance imaging · T_1 contrast agent · Fe_8 · Iron phosphate particles

Introduction

Magnetic resonance imaging (MRI) is one of the most powerful techniques in clinical diagnostic medicine and in non-invasive biomedical research and has fostered the development of agents designed to enhance tissue differentiation in vivo. The effect of these agents, mainly complexes of Gd^{3+}, Fe^{3+}, and Mn^{2+}, is known to improve contrast in MR-based images (1,2). MRI contrast agents (CA) act by accelerating the relaxation process of water protons in tissues by selectively decreasing both the

E. Rodríguez (✉)
Institut de Ciència de Materials de Barcelona
(ICMAB-CSIC), Campus UAB,
08193 Bellaterra, Spain
e-mail: evrodriguez@partners.org

R. V. Simoes
Centro de Neurociências e Biologia Celular,
Universidade de Coimbra,
Coimbra, Portugal

R. V. Simoes · C. Arús
Departament de Bioquímica i Biologia Molecular,
Universitat Autònoma de Barcelona, Campus UAB,
08193 Bellaterra, Spain

A. Roig · E. Molins
Institut de Ciència de Materials de Barcelona
(ICMAB-CSIC), Campus UAB,
08193 Bellaterra, Spain

N. Nedelko · A. Ślawska-Waniewska
Institute of Physics Polish Academy of Sciences,
Al. Lotnikow 32/46, 02-668, Warszawa, Poland

S. Aime
Dipartamento de Chimica IFM, Università di Torino,
10125 Turin, Italy

M. E. Cabañas
Servei de RMN, Universitat Autònoma de Barcelona,
Campus UAB, 08193 Bellaterra, Spain

C. Sanfeliu
Institut d'Investigacions Biomèdiques de Barcelona
(CSIC-IDIBAPS), 08036 Barcelona, Spain

S. Cerdán · M. L. García-Martín
Instituto de Investigaciones Biomédicas "Alberto Sols"
(UAM-CSIC), Madrid, Spain

longitudinal relaxation time, T_1, and the transversal relaxation time, T_2. Gd^{3+} complexes have received most attention as contrast agents for MRI applications due to their large magnetic moment and a suitable long electronic relaxation time. However, there is no natural human biochemistry for Gd^{3+} that can be exploited when designing its contrast agents derivates (3–6). On the other hand, agents based on Mn^{2+}, Fe^{3+}, and Cu^{2+} ions are attractive alternatives (7–9) because these metals are already present in tissues and there is extensive information available about their human biochemistry, including transport, storage, compartmentalization and excretion mechanisms. Many of the iron-based contrast agents consist of superparamagnetic particles of colloidal iron oxides that cause T_2-enhancement (10,11). A second type of iron-based contrast agents are iron(III) mononuclear complexes. In this case the ligands provide coordinative saturation to the iron, avoiding the occurrence of Lewis acid-catalyzed hydrolysis reactions and redox processes (12), toxic to the body and which are potentially facilitated by free Fe^{3+} ions. Furthermore, Fe^{3+} ions must be chelated to avoid precipitation caused losses near pH ∼7.

The complex $[(tacn)_6Fe_8(\mu_3\text{-}O)_2(\mu_2\text{-}OH)_{12}]Br_8 \cdot 9H_2O$, where tacn = 1,4,6-triazacyclononane, and hereafter referred to as Fe_8, was chosen by us in order to study its potential as contrast agent (13). Due to the size of Fe_8 molecules, the distribution and residence time in the tissues should be different and produce complementary information to that given by Gd-based chelates and iron oxide nanoparticles. A major shortcoming of clinical and experimental MR contrast agents is that they are limited to reporting anatomic detail only. Nevertheless, significant progress has been made on the design and preparation of MR agents that are brighter, selectively targeted and have a longer residence time in vivo (14,15).

In this work, we present the unexpected relaxometric properties of the solutions obtained by adding a known amount of the Fe_8 molecule to phosphate salt solutions at different concentrations of K_2HPO_4, and hereafter referred as $Fe_{(phos)}$. Spectroscopic and magnetic studies of the $Fe_{(phos)}$ solutions were also carried out. The results have shown the instability of the Fe_8 precursor in phosphate solutions and the formation of a new time-stable species, $Fe_{(phos)}$, rapidly established among the Fe^{3+} ions and amine ligands present in the Fe_8 cluster and phosphate ions. Therefore we hypothesized that the new contrast agent described in this work could be potentially useful to report on hyperphosphatemic regions inside a living organism. Before embarking in such a study, in vivo effect and tolerance need to be assayed. For this, toxicity studies of $Fe_{(phos)}$ solutions using C6 glioma cells were carried out. Furthermore, preliminary in vivo studies were also performed with mice to evaluate both toxicity, with control animals, and T_1 contrast enhancement for stereotactically induced brain tumours.

Experimental section

Synthesis of $[(tacn)_6Fe_8(\mu_3\text{-}O)_2(\mu_2\text{-}OH)_{12}]Br_8 \cdot 9H_2O$

Reagents were purchased from Sigma Aldrich (Spain) and used as received without further purification. The synthesis of Fe_8 was performed as described by Wieghardt et al. (16). A special batch enriched with ^{57}Fe isotope was prepared to be used for the Mössbauer characterization.

NMR relaxation studies

^1H measurements were performed on a Bruker Avance 300 spectrometer operating at a magnetic field of 7.0 T at 298 K. Inversion-recovery (180°_x-τ-90°_x-acquire) and Carr-Purcell-Meiboom-Gill (90°_x-[τ-180°_y-τ]$_n$-acquire) pulse sequences were used to measure T_1 and T_2, respectively. Five millimeter-diameter NMR tubes, each containing deuterated water (used for locking purposes) and a capillary tub insert filled with the iron aqueous solutions, were used essentially as in (13). Relaxation time constants were obtained by fitting the proper equation to the peak area data using a least-squares algorithm as implemented in the processing Bruker software. Correlation coefficients greater than 0.9 were obtained in all cases.

T_1 relaxation measurements at 0.24 T and 298 K were performed on a Spinmaster FFC, fast field cycling, Stelar, in the following range 0.00024–0.24 T. Three independent experiments were measured for each concentration, and each data point corresponds to one experiment.

$Fe_{(phos)}$ solutions were prepared with 2 mg/ml of Fe_8 in phosphate solutions ranging from 0.01 to 1 M of K_2HPO_4 salt, at neutral "(7)" and basic "(12)" pH. Relaxivities values are referred to moles of Fe, where 1 mM Fe_8 equals 8 mM Fe.

Spectroscopic and magnetic characterization

^{31}P spectra of $Fe_{(phos)}$ were performed on a Bruker Avance300 spectrometer operating at a magnetic field of 7.0 T, at 298 K with 5 mm tubes. Spectra of the $Fe_{(phos)}$ were obtained from four samples of a solution 0.5 ml of 10 mg/ml of Fe_8 in 0.005, 0.01, 0.25 and in 1 M aqueous

phosphate solutions, respectively, at neutral pH ($7 < pH < 7.4$). ^{31}P spectrum of the K_2HPO_4 salt in aqueous solution was also recorded. ^2H_2O was used for locking purposes and H_3PO_4 (85%) as external reference.

Mössbauer spectra of $Fe_{(phos)}$ and the Fe_8 powder, hereafter referred as $Fe_{8(s)}$, were recorded at 4.2 K with a conventional transmission spectrometer using a ^{57}Co source in Rh matrix. Calibration was carried out using a 25-μm thick natural iron foil. Spectra of the $Fe_{(phos)}$ were obtained from two samples of a frozen solution 0.5 ml of 10 mg/ml of $^{57}Fe_8$ in 0.05 M and in 1 M phosphate solutions, respectively, at neutral pH.

The temperature dependences of dc magnetization for the frozen phosphate solution and the $Fe_{8(s)}$, samples were measured with a PPMS magnetometer (Quantum Design) over the temperature range 2–250 K in an applied field up to 90 kOe. The experimental results were corrected for the holder contribution as well as for a temperature independent diamagnetic contribution. For the magnetic studies two solutions of 10 mg/ml of Fe_8 in 0.05 and 1 M were prepared at neutral pH. All the magnetization data are presented in emu/mol Fe.

Cells and animals

The C6 cell line from rat glioma was obtained from the European Collection of Cell Cultures (ECACC). Cells were maintained in Ham's F-12 supplemented with 10% foetal bovine serum, 2 mM glutamine and 50 μM gentamicin. C6 glioma cells were grown in culture flasks and passed every 3–4 days. GL261 mouse glioma cells were obtained from the Tumour Bank Repository at the National Cancer Institute, Frederick, USA and constitute a well-established experimental glioma model in mice (17). These were grown in RPMI-1640 culture medium supplemented with 2.0 g/l sodium bicarbonate, 0.285 g/l L-glutamine, 10% foetal bovine serum (*Gibco*) and 1% penicillin–streptomycin Solution. Culture medium and chemicals were purchased from Sigma unless otherwise indicated. Culture plastic was obtained from Nunc.

Thirty CD1 mice (Charles-River Labs., France) with weights between 24 and 36 g, were used for toxicity studies. MRI studies were performed with mice harbouring a brain tumour, which is a classic pathology model to demonstrate T_1 contrast effect in vivo (18). For this we implanted a total of seven mice with murine glioma cells: six with GL261 cells (mice 1–6) (18) and one with C6 cells (mouse 7) (19). Briefly, animals were anesthetized intraperitoneal (i.p.) with ketamine–xylasine, 80–10 mg/kg, and then immobilized on a stereotactic holder (Kopf Instruments, Tujunga, CA, USA). After the scull was exposed, a 1.0 mm hole was made 2.3 mm lateral (right) to the midline, as measured from the *Bregma*. A 26G Hamilton syringe (Reno/NV, USA), positioned on a digital push-pull microinjector (Harvard Apparatus, Holliston, MA, USA) was then advanced 2.3 mm from the cortical surface into the *striatum*, and 4 μl RPMI medium containing 10^5 GL261 (or C6) cells were injected at a rate of 2 μl/min. Three to five minutes after the injection had finished, the syringe was slowly removed, the scission site closed with suture silk (5.0) and the animal left to recover in a warm environment (about 25°C). Toxicity studies were conducted at the animal facility of the University of Barcelona, where animals were housed. For in vivo tumour studies, animals were housed first at the animal facility of Universitat Autònoma de Barcelona (Servei d'Estabulari), where tumour cells were stereotactically injected, and then transported to the *Instituto de Investigaciones Biomedicas "Alberto Sols"* UAM-CSIC, Madrid, where MR studies were conducted. Animals were always fed ad libitum, allowed 12–12 h light–dark cycles and were treated according to protocols approved by the animal healthcare committee of each relevant institution.

Toxicity studies

In vitro

For cytotoxicity assays, cells from the C6 glioma cell line were seeded in 12-well plates and treated for 72 h with the $Fe_{(phos)}$. We used the lactate dehydrogenase (LDH) leakage test that indicates the presence of cell membrane damage (20). In a previous work we have determined the reliability of LDH test for analyzing Fe_8 cytotoxicity (13). Using a spectrophotometric NADH consumption assay, in the presence of pyruvic acid substrate, LDH leaked from cells was measured in the culture medium after 72 h exposure to $Fe_{(phos)}$ solutions and expressed as the change in optical density per min (ΔOD/min).

In vivo

According to spectroscopy and magnetic characterization results obtained previously in vitro (see Results section), $Fe_{(phos)}$ solutions were prepared at a ratio $[HPO_4^{2-}]/[Fe_8]$ of 10, pH 7.2. In vivo toxicity of these $Fe_{(phos)}$ solutions was evaluated in CD1 mice. Different dose levels were administrated by intravenous (i.v.) tail injection with a volume of 4 μl/g. The study was performed with groups of five males and five females per dose. Animals were regularly monitored for two weeks

after the injection of $Fe_{(phos)}$. After that, all surviving animals were sacrificed and autopsied.

MRI studies

Seven mice harbouring a brain tumour were used for MRI studies. These were carried out at 7.0 T on a Bruker *PharmaScan* 70/16 (SIERMAC, UAM-CSIC), equipped with active shielded gradients, 300 mT/m, and a 30-mm proton RF coil, optimized for the mouse head. Anaesthesia was performed with isoflurane at 1–2.5% in O_2 and the respiratory frequency maintained between 40 and 60 breaths/min. Animals were also thermostatized with a heated water blanket during this procedure. Before immobilization in the MR holder each animal was canulated in the tail vein (i.v.) with a 26G Abbocath-T. For both, animal scanner time economy and to be able to compare the differential effect of the two contrast agents, avoiding at the same time potential interferences of different tumour vascularization on each animal, both $Fe_{(phos)}$ and Gd-DTPA were used in the same experiment with each animal. After detecting each tumour by T_2 weighted imaging, Dynamic contrast enhanced T_1 (DCE-T_1) MRI was performed in the slices of interest along with the *iv* bolus injection of either Gd-DTPA or $Fe_{(phos)}$ solution, both at 4 μl/g. Assuming an approximate 1:11.8 dilution of each contrast agent when spreading into the blood pool of each mice after injection (calculations explained in more detail ahead in the Discussion section), the $Fe_{(phos)}$ dose used in these studies was always kept below those described as non-toxic from both in vivo and in vitro toxicology analysis (1 mM and 0.04 mmol/kg, respectively, see Results section). Order of injection in mice harbouring GL261 tumours was $Fe_{(phos)}$ (0.04 mmol Fe_8/kg) followed by Gd-DTPA (mice 1–5: 0.2 mmol/kg; mouse 6: 0.04 mmol/kg) after 2 h 30 min–3 h washout period. As for mouse 7, implanted with C6 cells, Gd-DTPA was injected first (0.2 mmol/kg) and, 4 h later, the $Fe_{(phos)}$ solution (0.04 mmol Fe_8/kg). In all cases, the second contrast agent was not injected until there was a visual washout confirmation of the previous one in T_1 control images. Acquisition parameters for T_2 weighted images were: RARE sequence; turbo factor, 8; field of view (FOV), 20 × 20 mm; matrix (MTX), 256 × 256 (78 × 78 μm/pixel); number of slices (NS), 14; slice thickness (ST), 1 mm; interslice-thickness (IST), 1.1 mm TR/TE = 2,500/60 ms; number of averages (NEX), 4; total acquisition time (ACQ), 5 m 20 s. For DCE-T_1: MSME sequence; FOV, 21 × 21 mm; MTX, 128 × 128 (164 × 164 μm/pixel); NS, 3; ST, 1 mm; IST, 1.1 mm; TR/TE, 200/9 ms; NEX, 1; number of images acquired for each slice (NR), 40; ACQ, 34 m 8 s (51 s 200 ms per slice group episode); bolus injection of the CA during acquisition of the second image. DCE-T_1 images were then processed with IDL (RSI, France) home written scripts to generate time-course curves that quantified the average contrast enhancement inside the tumours (defined from regions of interest, ROIs). ImageJ freeware software was also used to obtain fusion images (T_2 control images overlapped with colour coded CE-T1 data).

Results

NMR relaxometric studies

The dependence of relaxivities r_1 and r_2 with the concentration of K_2HPO_4 for a given initial Fe_8 concentration of 1 mM (8 mM of Fe) at 7.0 T is shown in Fig. 1. The T_1 and T_2 values were converted to relaxivity in $mM^{-1}\,s^{-1}$ Fe by taking into account the dilution factor used. An increase of r_1 and r_2 was observed as the concentration of phosphate salt increased. The time stability of the r_1 and r_2 values was checked by repeating the r_1 and r_2 measurements at several times (2, 8, 24 and up to 100 h). While no relaxivity time changes were observed for a K_2HPO_4 to Fe_8 molar ratio, $[HPO_4^{2-}]/[Fe_8]$, equal or higher than 10, for lower concentrations of K_2HPO_4, r_1 and r_2 values decreased with time (results not shown). The dependence of r_1 with the K_2HPO_4 concentration at 0.24 T has been measured at basic and neutral pH values (see inset in Fig. 1). The r_1 value at basic pH

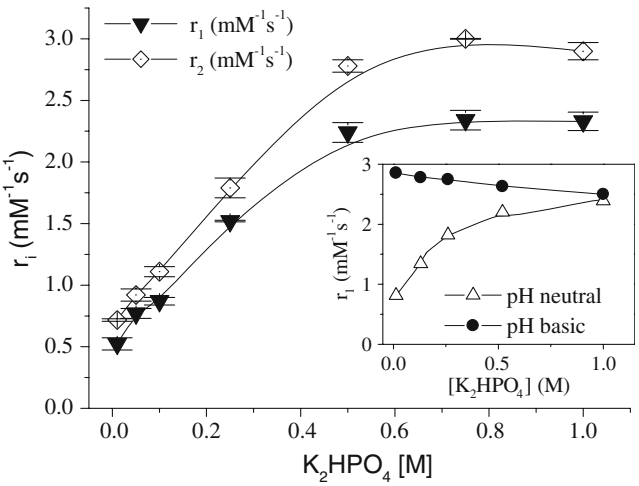

Fig. 1 Relaxivities, r_1 and r_2, dependence with the concentration of K_2HPO_4 for a given initial Fe_8 concentration of 1 mM at 7.0 T and 298 K. Three independent experiments were measured for each concentration, and each data point corresponds to one experiment. r_1 dependence with the concentration of K_2HPO_4 at 0.24 T at pH values of 7 and 12 is shown in the inset

is essentially constant for all phosphate concentrations and has a value comparable with the maximum achieved at neutral pH. The different behavior of r_1 at basic and neutral pH values is more evident for lower K_2HPO_4 concentrations such as $[HPO_4^{2-}] = 0.01\,M$, where the r_1 value increases from $0.8\,mM^{-1}\,s^{-1}$, at neutral pH, to $2.8\,mM^{-1}\,s^{-1}$, at a basic one.

Spectroscopic and magnetic characterization

Spectroscopic and magnetic characterization were carried out in order to increase our understanding of the type of interaction of the phosphate ligands and the iron ions in $Fe_{(phos)}$. For this purpose several solutions with different $[HPO_4^{2-}]/[Fe_8]$ ratios were prepared. ^{31}P spectra of these solutions are shown in Fig. 2. As the K_2HPO_4 concentration increases, there is a rise in the apparent peak intensity at about 2.5 ppm with respect to baseline noise, which corresponds to free K_2HPO_4. Nevertheless, for ratios of $[HPO_4^{2-}]/[Fe_8]$ lower than ten, no resonance was detected suggesting a strong interaction between the phosphate ligands and the iron ions.

Moreover, for a given initial concentration of Fe_8 the magnetic properties and Mössbauer spectroscopy of two $Fe_{(phos)}$ samples, with low (0.05 M), $[HPO_4^{2-}]/[Fe_8] = 10$, and high (1 M), $[HPO_4^{2-}]/[Fe_8] = 500$, concentration of phosphate salt were carried out. Mössbauer spectra of $Fe_{(phos)}$ at 4.2 K are shown in Fig. 3a and b. In the same manner, Mössbauer spectrum of the powered sample, $Fe_{8(s)}$, was recorded for comparison (Fig. 3c). The differences between the three spectra are evident. For 0.05 M K_2HPO_4 (Fig. 3a) the spectrum could be fitted using two symmetrical doublets while for 1 M K_2HPO_4 (Fig. 3b) the spectrum could be fitted using three subspectra; two symmetric doublets and a magnetically split sextet accounting for about 25% of the total area. On the contrary, the precursor molecule $Fe_{8(s)}$ (Fig. 3c) shows a completely resolved spectrum indicating that all spins are frozen in a collective state and no paramagnetic

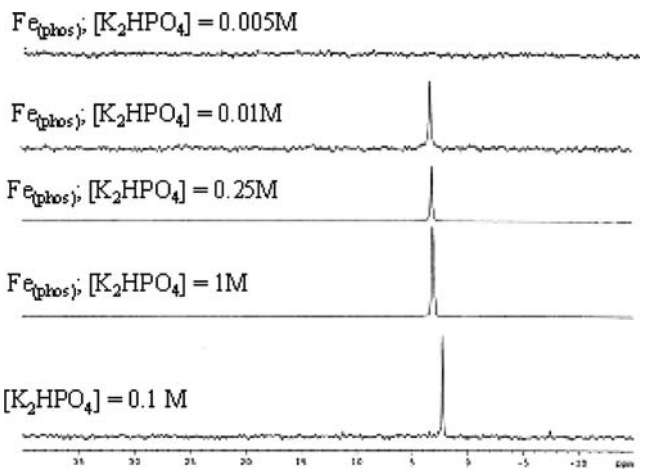

Fig. 2 ^{31}P spectra of $Fe_{(phos)}$ solutions with $[K_2HPO_4] = 0.005, 0.01, 0.25$ and 1 M, respectively and of 0.1 M K_2HPO_4 salt at 7.0 T, 298 K and at neutral pH ($7 < pH < 7.4$)

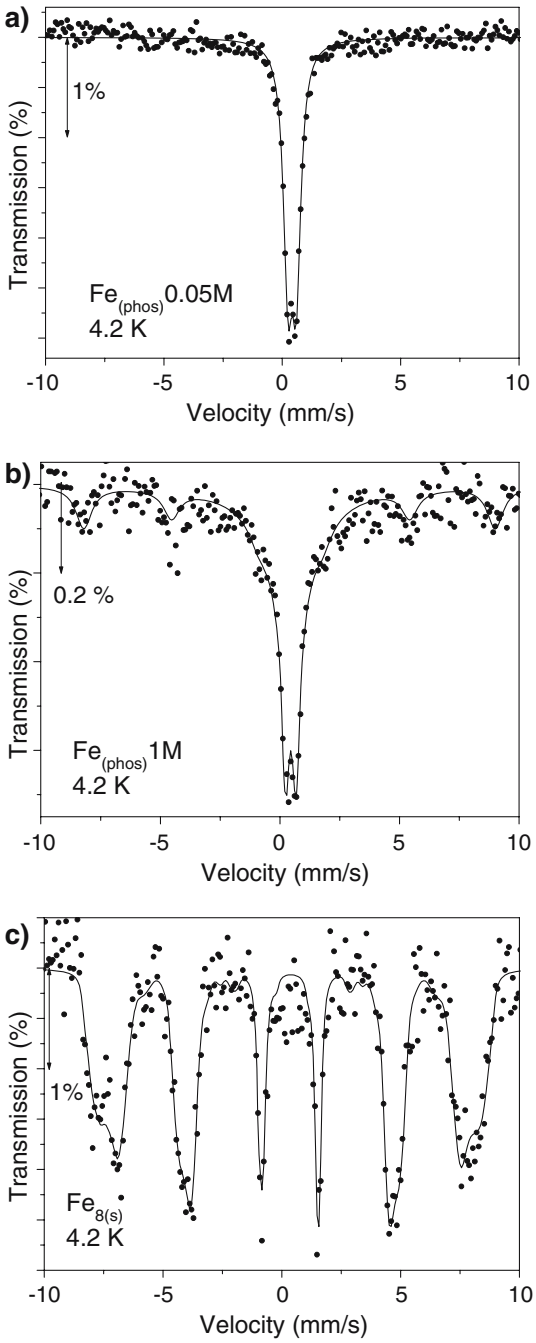

Fig. 3 Mössbauer spectra for $Fe_{(phos)}$ and $Fe_{8(s)}$ at 4.2 K; **a** corresponds to $Fe_{(phos)}$ for concentration $[K_2HPO_4] = 0.05\,M, [HPO_4^{2-}]/[Fe_8] = 10$; **b** corresponds to $Fe_{(phos)}$ for concentration $[K_2HPO_4] = 1\,M, [HPO_4^{2-}]/[Fe_8] = 500$ and **c** corresponds to $Fe_{8(s)}$

phase, that would lead to a central doublet, or singlet is detected. The results obtained from Mössbauer spectroscopy for the two $Fe_{(phos)}$ samples suggest: (1) in both cases the iron is found as Fe^{3+} species, and (2) for the low phosphate sample, 0.05 M K_2HPO_4, a typical paramagnetic or superparamagnetic behaviour is observed while for the concentrated sample, 1 M K_2HPO_4, a fraction of the iron ions (25%) becomes magnetically coupled at low temperatures in agreement with the formation of an oligomeric species (21). Magnetic characterization was carried out to complement Mössbauer spectroscopy. The temperature dependences of χT for $Fe_{(phos)}$ solutions, for 0.05 M K_2HPO_4 and 1 M K_2HPO_4, obtained in a field of 90 kOe are shown in Fig. 4a, b, which suggest an antiferromagnetic coupling between Fe ions for both samples. For the powered sample, $Fe_{8(s)}$, the $\chi T(T)$ curve measured at 90 kOe is also shown in Fig. 4c. χT values exhibit a plateau at elevated temperatures, then a steadily increase on decreasing temperature up to a certain maximum followed by a rapid decrease indicating that the Fe^{3+} clusters have ferrimagnetic spin ordering. Thus, $\chi T(T)$ dependence obtained for $Fe_{8(s)}$ is very different from those obtained for $Fe_{(phos)}$ solutions pointing to a re-arrangement of the Fe^{3+} ions in the phosphate solution and the appearance of antiferromagnetic coupling between Fe ions.

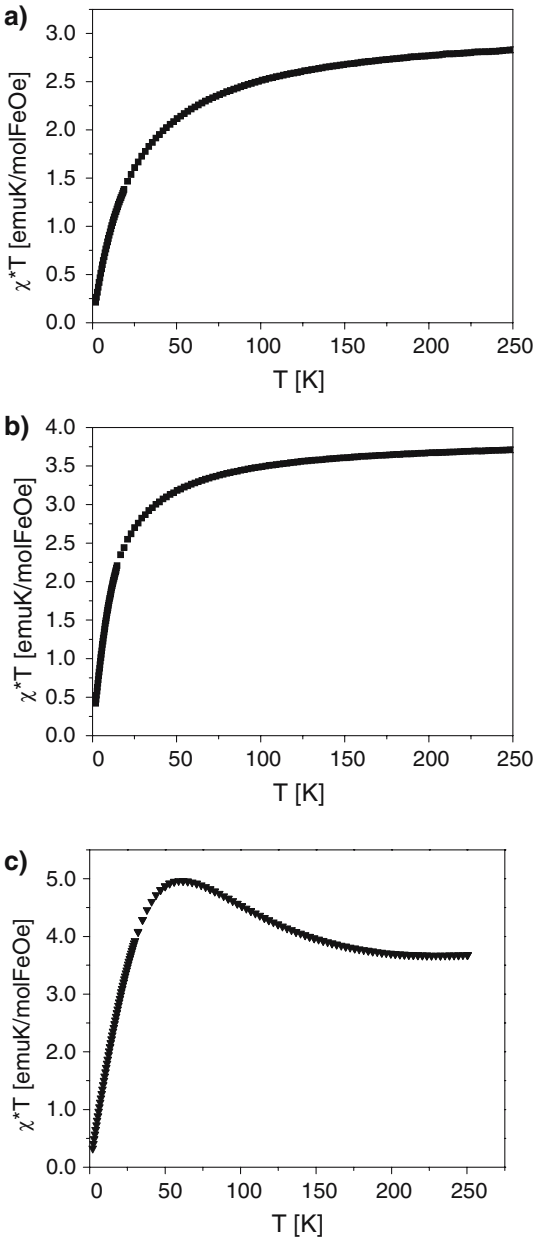

Fig. 4 Temperature dependence of the susceptibility measured at H = 90 kOe-$\chi_g T$ versus T for: **a** $Fe_{(phos)}$ for concentration $[K_2HPO_4] = 0.05\,M, [HPO_4^{2-}]/[Fe_8] = 10$; **b** $Fe_{(phos)}$ for concentration $[K_2HPO_4] = 1\,M, [HPO_4^{2-}]/[Fe_8] = 500$ and **c** $Fe_{8(s)}$

Toxicity studies

Hereafter the $Fe_{(phos)}$ doses used for the described studies have been prepared maintaining a ratio $[HPO_4^{2-}]/[Fe_8] \geq 10$, in order to assure the stability of the newly formed complex in aqueous solution.

In vitro

The effects of $Fe_{(phos)}$ treatment on cell viability in the C6 glioma cell line were studied after exposures of 72 h duration. For this, the standard cell culture medium was replaced by media containing the $Fe_{(phos)}$ solutions. The range of concentrations of Fe_8 studied was 0.1–1 mM and the concentration of phosphate added was 10 mM. Stock solutions pH was adjusted to neutral pH. Figure 5 shows the LDH released by increasing mM concentrations of Fe_8. No cytotoxicity effects of $Fe_{(phos)}$ were detected in C6 cell cultures in the whole range of concentrations tested.

In vivo

The toxicity assay of $Fe_{(phos)}$ solution in mice after i.v. injection was performed at doses of 0.04, 0.06 and 0.08 mmol Fe_8/kg body weight, and the concentrations of phosphate added were 0.4, 0.6 and 0.8 mmol/kg, respectively. The lower dose resulted in 100% survival (ten animals); the middle dose resulted in 80% survival (four animals out of five of each sex survived); and the higher dose tested resulted in 60% survival (three animals out of five of each sex survived). Death happened either briefly after the injection when preceded by convulsion or it was delayed several days and then preceded by

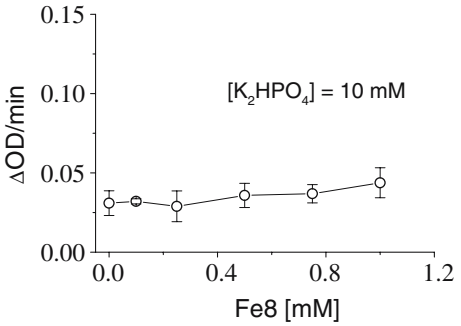

Fig. 5 Concentration–response cytotoxicity curves. LDH leaked from the cells in the presence of $Fe_{(phos)}$ solutions, with 10 mM of K_2HPO_4 added. Three independent experiments were measured for each concentration, and each data point corresponds to one experiment

a period with activity depression, ataxia and reduced animal response to stimulation. No significant abnormal findings were observed at the macroscopic autoptic analysis for any of the sacrificed animals.

MRI studies

As shown in Fig. 6, all DCE-T1 studies performed with $Fe_{(phos)}$ solutions produced a positive contrast-enhancement in brain tumours, both for GL261 (mice 1–5, 12 time-course curves: maximum 114±5%—Fig. 6a; mouse 6, 3 time-course curves: maximum 118 ± 3%—Fig. 6b) and for C6 (mouse 7, 3 time-course curves: maximum 123 ± 9%—Fig. 6c), as compared to reference T_1 control images (100%). This is shown with CE-T1 images (III), fusion images (IV) and also with the time-course curves for each contrast agent (V) presented all together in Fig. 6. Nevertheless, this effect was always inferior to that obtained with Gd-DTPA, either at the standard dose (mice 1–5 and mouse 7, 0.2 mmol/kg: 177 ± 17% and 184 ± 21%, respectively), or at an equivalent dose to that of $Fe_{(phos)}$ (mouse 6, 0.04 mmol/kg: 130 ± 2%). Also, in most GL261 tumour cases studied the contrast enhancement achieved with the $Fe_{(phos)}$ solution was not well distinguished visually after the first minutes post-injection despite being well observed in the time-course curves. The only exception was the single C6 tumour studied, where apparently the washout period of the $Fe_{(phos)}$ solution was much longer. Moreover, Fig. 7 shows the time-course of the intensity measured in ROIs positioned in the jugular veins (interior and exterior) after bolus injection of each contrast agent. Despite the large standard deviations, it is possible to observe a slightly larger signal enhancement with Gd-DTPA during the initial minutes post-injection (at 1.8 min: 211 ± 121% with Gd-DTPA and 161 ± 42% with $Fe_{(phos)}$ solution) becoming at later times indistinguishable among the two compounds, albeit Gd-DTPA seems to display a tendency to faster clearance from blood than $Fe_{(phos)}$.

Discussion

In this work, we have characterized the relaxometric properties of the Fe^{3+} ions, originated from the rearrangement of the Fe^{3+} ions from the initial cation $[(tacn)_6Fe_8(\mu_3\text{-}O)_2(\mu_2\text{-}OH)_{12}]^{8+}$, $[Fe_8]^{8+}$, and the phosphate groups present in phosphate solutions. To our surprise, for a given initial concentration of Fe_8, the T_1 and T_2 relaxation times of water protons notably dropped as the concentration of phosphate was increased. For instance, as the ratio $[HPO_4^{2-}]/[Fe_8]$ was changed from 10 to 1,000, r_1 increased from 0.5 $mM^{-1}s^{-1}$ to 2.5 $mM^{-1}s^{-1}$. Furthermore, it was determined that the ratio $[HPO_4^{2-}]/[Fe_8]$ must be equal or higher than ten in order to obtain time-stable relaxometric results. For a given concentration of Fe_8, the large r_1 values obtained at basic pH and its lack of dependence of the phosphate/Fe_8 ratio suggests a possible role of the PO_4^{3-} species in complex formation with the Fe^{3+} ions. Nevertheless, further measurements should be performed to corroborate this assumption. Spectroscopic and magnetic measurements of $Fe_{(phos)}$ confirmed that the Fe_8 molecule does not remain stable in phosphate solution. These studies also suggested that the decomposition is catalysed by the phosphate group, and it is followed by formation of a stable, possibly colloidal, suspension of oligomeric species which composition and size is likely to depend on the ratio between Fe and phosphate. It should be pointed out that no precipitation was observed at any pH value or $[HPO_4^{2-}]/[Fe_8]$ ratio studied. This is indicative that the amine groups are present in the final product, since otherwise Fe^{3+} hydroxides would have precipitated, which was not the case. A possible explanation for the observed increase of relaxivity values at neutral pH as the phosphate concentration is increased could be that the phosphate anion allows the formation of a short-lived second coordination complex where these phosphate ligands promote an approximation of the water protons to the Fe^{3+} ions. This dynamic process would be based in the fast exchange of water molecules near physiologic pH with the complex, which would allow this relaxivity increase. Increasing the phosphate concentration would enhance the formation of an oligomeric species which in turn, would result in a decrease of its rotational time. To validate our model, the resolution of the crystal structure of the new compound in the

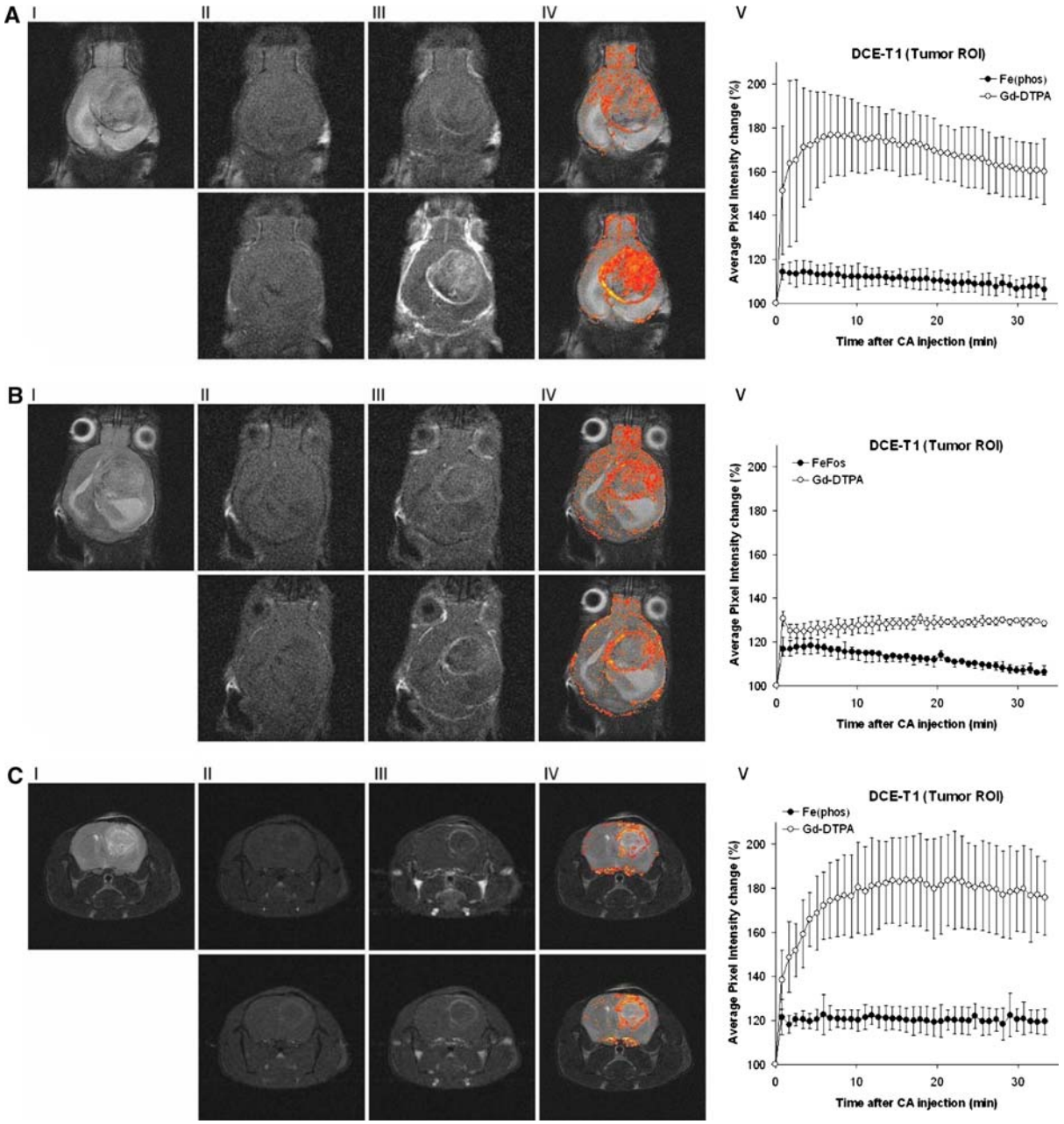

Fig. 6 In vivo MRI studies. Column I, *T*2 images of the brain highlighting the tumour. Sections are transversal in A and B and coronal in C. Columns II and III, DCE-*T*1 studies: control *T*1 images previous to bolus injection (II) and first CE-*T*1 images acquired in the study at 51 m 200 s post-injection (III). Column IV, fusion of image I with a colour-coded reconstruction of image III that shows the signal enhancement (*red*, lowest, to *yellow*, highest) only inside the brain. Column V, time–course curves showing the average signal enhancement in the tumour region (manually defined by ROIs) after bolus injection of each contrast agent. **a** Mouse harbouring a GL261 brain tumour studied first with $Fe_{(phos)}$ 0.04 mmol/kg (II–IV, *upper row*) and, 2 h later, with Gd-DTPA 0.2 mmol/kg (II–IV, *bottom row*). Time–course curves represent the average readings from different slices in mice 1–5 (12 time–course curves for each contrast agent). **b** Mouse harbouring a GL261 brain tumour studied first with $Fe_{(phos)}$ 0.04 mmol/kg (II–IV, *upper row*) and, 3 h later, with Gd-DTPA 0.04 mmol/Kg (II–IV, *bottom row*). Time–course curves represent the average readings (bar ± SD) from three slices in mouse 6 (three time–course curves for each contrast agent). **c** Mouse harbouring a C6 brain tumour studied first with Gd-DTPA 0.2 mmol/kg (II–IV, *upper row*) and, 4 h later, with $Fe_{(phos)}$ 0.04 mmol/kg (II–IV, *bottom row*). Time–course curves represent the average readings (bar ± SD) from three slices in mouse 7 (three time–course curves for each contrast agent)

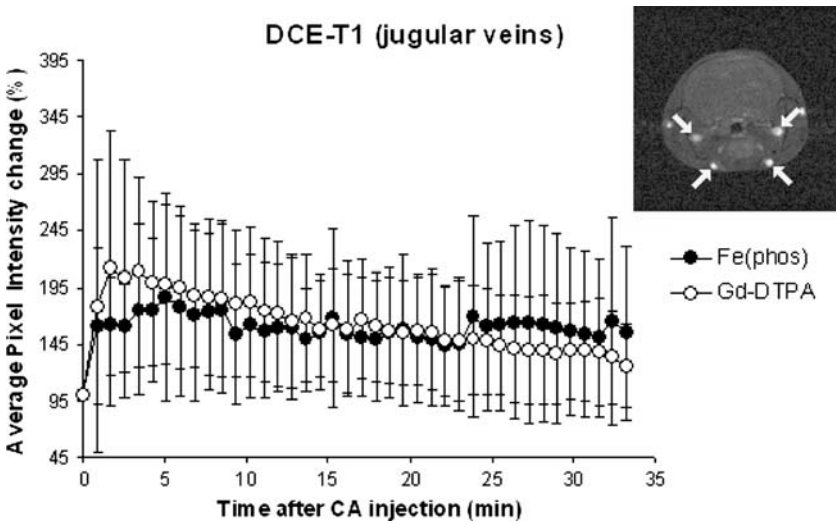

Fig. 7 Average time time–course (bar ± SD) of the intensities measured in ROIs positioned in the jugular veins (interior and exterior, highlighted by *white arrows* on the CE-T1 image obtained with $Fe_{(phos)}$ solution) after bolus injection of each agent (CA) in four animals implanted with GL261 cells (four ROIs per animal produce a total of 16 curves)

presence of phosphate groups would be of great help. However, in spite of the large number of attempts made using several strategies no acceptable crystals were obtained.

It may be relevant to mention here early work (27) in which a polynuclear Fe(III) · ATP (4:1) stable complex in solution was demonstrated. The molecular weight of that complex was in excess of 50,000 M_r and, as in the case for $Fe_{(phos)}$ at $[HPO_4^{2-}]/[Fe_8] \leq 10$, ^{31}P NMR resonances for ATP were broadened beyond detection, presumably due to paramagnetic interaction of the phosphate resonances of ATP with Fe(III). In this Fe(III) · ATP complex the N of the purine ring seemed to participate in complex stabilization. A similar role could be playing in the $Fe_{(phos)}$ complex herewith studied the N atoms contributed by the tacn.

Cytotoxicity studies showed lack of toxic effects for a ratio of $[K_2HPO_4]/[Fe_8] \geq 10$, suggesting that there are no free iron(III) ions in the phosphate solution in contrast with their presence detected in aqueous solutions in which phosphate was absent (22). Our preliminary DCE-T1 MRI studies obtained in vivo demonstrate that $Fe_{(phos)}$ solutions produce positive contrast enhancement in glioma brain tumours grown in mice at a dose that presented no toxic effects up to 14 days post-injection in control animals. Nevertheless, Gd-DTPA is clearly more efficient as a contrast agent to highlight blood-brain barrier (BBB) breakdown in brain tumours than the $Fe_{(phos)}$ solution, producing about five times more contrast at the highest doses tested here. Taking into account the fact that both agents produced an identical signal enhancement in the vascular bed, as described in Fig. 7, the lower enhancement of tumour contrast produced by $Fe_{(phos)}$ could possibly be due to a decrease in the inorganic phosphate (Pi) concentration in the extracellular tumour compartment with respect to the Pi concentration in the mouse plasma. In this respect, Pi concentrations described in the literature for mouse plasma is in the 0.82–3.08 mM range (average 1.95 mM), calculated from (23,24). Furthermore, after $Fe_{(phos)}$ i.v. injection (4 μl/g) the plasma Pi levels are expected to rise to about 10.45 mM (assuming 1.1 ml of plasma in a 25 g mouse and an average basal plasma Pi of 1.95 mM). Simultaneously the iron (Fe_8) concentration in plasma coming from $Fe_{(phos)}$ injection would be expected to be about 0.85 mM, therefore producing a $Pi/Fe_{(phos)}$ ratio higher than ten. This should produce, as described in the NMR relaxometric studies section, high r_1 values and optimal positive contrast enhancement, as demonstrated from venous blood in Fig. 7. On the other hand, results shown in Fig. 6 would be coherent with a much lower Pi concentration in the tumour extracellular fluid than in circulating blood causing a decreased effect on water relaxivity and, thus, lower contrast enhancement. Nevertheless, it may be relevant to compare results obtained with GL261 and C6 cells. C6 derived rat glioma tumours are know to be very necrotic (25). Furthermore, the species difference for cells (C6, rat) and host (mice) in this work would be expected to generate an immune response with concomitant macrophage invasion which could also further increase tumour necrosis. All tumours shown in Fig. 6 had apparent necrotic regions as may be deduced from CE-T1 and fusion images by the typical "ring enhancement" pattern seen (18), using both contrast agents. Furthermore, those tumours appear to contain poorly perfused regions as pointed by the selective slow entry of Gd-DTPA in such areas (as found in time-course curves, results not shown). As expected, the single C6 tumour studied appeared to be more necrotic (slower entry

and longer washout time for Gd-DTPA) than GL261 tumours, with some positive contrast already observed in the control T_1 images. In agreement with this, the $Fe_{(phos)}$ solution produced higher and longer lasting contrast enhancement in the C6 tumour than in any of the GL261 tumours studied. This result could be interpreted as due to higher extracellular Pi the more necrotic the tumour is. In this respect, it may be of interest to investigate the performance of $Fe_{(phos)}$ under conditions in which hyperphosphatemia is expected, e.g., in the Tumour Lysis Syndrome (TLS), situation which normally follows chemotherapy treatment of tumours (26), or for cell tracking applications (28,29), due to the fact that intracellular Pi concentration is normally much higher than extracellular Pi.

Conclusions

$Fe_{(phos)}$ solutions present interesting relaxometric properties. For a given initial concentration of Fe_8, and by varying the concentration of the phosphate salt, the r_i value increases to maximal values of $r_1 = 2.5$ and $r_2 = 2.9\,mM^{-1}s^{-1}$ for a $[HPO_4^{2-}]/[Fe_8] = 1,000$. Magnetic measurements of $Fe_{(phos)}$ solutions show that the initial Fe_8 molecule is not stable and that the phosphate concentration plays an essential role in the final stability and relaxometry properties of the new species. Only for ratios of $[HPO_4^{2-}]/[Fe_8] \geq 10$, the possible colloids that are present in solution are time-stable and its composition and/or size will depend on the concentration of the phosphate salt. In vitro and in vivo toxicity studies of $Fe_{(phos)}$ solutions confirm the lack of detectable toxic effects up to a concentration of 10 mM Fe_8/100 mM phosphate, suggesting that no toxic free iron ions are eventually released. We have also demonstrated that the $Fe_{(phos)}$ solution is well tolerated by mice at a concentration that enables positive T_1 contrast enhancement of brain tumours albeit less efficient than commercially available compounds, such as Gd-DTPA. The possible application of the $Fe_{(phos)}$ solution for highlighting in vivo hyperphosphatemic regions or its potential use in angiography or cell tracking deserves further investigation.

Acknowledgments The authors thank Patricia Sánchez for her help in inducing C6 tumours in mice and Carme Cleries for skilful technical assistance in toxicology studies. This work was funded by: *Ministerio de Ciencia y Tecnología* (MCYT SAF 2002-0440 and MCYT MAT 2003-01052), *Ministerio de Educación y Ciencia* (MEC SAF 2005-03650), *Fondo de Investigaciones Sanitarias* (2003-0467), *Fundação para a Ciência e a Tecnologia* (SFRH/BD/17643/2004).

References

1. Lauffer RB (1987) Paramagnetic metal complexes as water proton relaxation agents for NMR imaging: theory and design. Chem Rev 87:901–927
2. Merbach A, Tóth E, Helm T (2001) Relaxivity of gadolinium (III) complexes: theory and mechanism. In: Merbach A, Tóth E (eds.) The chemistry of contrast agent in medical resonance imaging. Willey-VCH, Chichester, pp 46–119
3. Caravan PJ, Ellison J, McMurry J, Lauffer RB (1999) Gadolinium (III) chelates as MRI contrast agents: structure, dynamics, and applications. Chem Rev 99:2293–2352
4. Aime S, Frullano L, Crich SG (2002) Compartmentalization of a gadolinium complex in the apoferritin cavity: a route to obtain high relaxivity contrast agents for magnetic resonance imaging. Angew Chem Int Edn 41:1017–1019
5. Laurent S, Vander Elst L, Yanjun F, Muller RN (2004) Synthesis and physicochemical characterization of Gd-DTPA-B(sLex)A, a New MRI contrast agent targeted to inflammation. Bioconjugate Chem 15:99–103
6. Geninatti S, Barge A, Battistini E, Cabella C, Coluccia S, Longo D, Mainero V, Tarone G, Aime S (2005) Magnetic resonante imaging visualization of targeted cells by the internalization of supramolecular adducts formed between avidin and biotinylated Gd^{3+} chelates. J Biol Inorg Chem 10: 78–86
7. Boudreau RJ, Frick MP, Levey RM, Lund G, Sirr SA, Loken MK (1986) The preliminary evaluation of Mn DTPA as a potential contrast agent for nuclear magnetic resonance imaging. Am J Physiol Imaging 1(1):19–25
8. Kupka T, Dziegielewski JO, Pasterna G, Malecki JG (1992) Copper-D-penicillamine complex as potential contrast agent for MRI. Magn Reson Imaging 10(5):855–858
9. Davies JA, Dutremez SG, Hockensmith CM, Keck R, Richardson N, Selman S, Smith DA, Ulmer CW, Wheatley LS, Zeiss J (1996) Iron-based second-sphere contrast agents for magnetic resonance imaging: development of a model system and evaluation of iron (III) tris (tironate) complex in rats. Acad Radiol 3(11):936–945
10. Colet J-M, Piérart C, Seghi F, Gabric I, Muller RN (1998) Intravascular and intracellular hepatic relaxivities of superparamagnetic particles: an isolated and perfused organ pharmacokinetics study. J Magn Reson 134:199–205
11. Artemov D., Mori N., Okollie B., Bhujwalla Z (2003) MR molecular imaging of the Her-2/neu receptor in breast cancer cells using targeted iron oxide nanoparticles. Magn Reson Med 49:403–408
12. Richardson N, Davies JA, Radüchel B (1999) Iron (III)-based contrast agent for magnetic resonance imaging. Polyhedron 18:2457–2482
13. Rodríguez E, Roig A, Molins E, Arús C, Quintero MR, Cabañas ME, Cerdán S, Lopez-Larrubia P, Sanfeliu C (2005) In vitro characterization of an Fe8 cluster as potential MRI contrast agent. NMR Biomed 18(5):300–307
14. Sirlin CB, Vera DR, Caballero MB, Buxton RB, Mattrey RF (2004) Gadolinium-DTPA-dextran a macromolecular MR blood pool contrast agent. Acad Radiol 11(12):1361–1369
15. Corot C, Robert P, Lancelot E, Martinell A, Santus R (2005) Distribution of gadomelitol in a human breast tumour model in mice. Magn Reson Mater Phy 18(3):138–143
16. Wieghardt K, Pohl K, Jibril I, Huttner G (1984) Hydrolysis products of the monomeric amine complex $(C_6H_{15}N_3)FeCl_3$: the structure of the octameric iron (III) cation of $\{[(C_6H_{15}N_3)_6Fe_8(\mu_3\text{-}O)_2(\mu_2\text{-}OH)_{12}]Br_7(H_2O)\}Br \cdot 8H_2O$. Angew Chem Int Ed Engl 1:77–78

17. Seligman AM, Shear MJ (1939) Studies in carcinogenesis. VIII. Experimental production of Brain tumors in mice with methylcholanthrene. Am J Cancer 37:364–395
18. Cha S, Johnson G, Wadghiri YZ, Jin O, Babb J, Zagzag D, Turnbull DH (2003) Dynamic, contrast-enhanced perfusion MRI in mouse gliomas: correlation with histopathology. Magn Reson Med 49(5):848–855
19. Rémy C, Arús C, Ziegler A, Lai ES, Moreno A, Le Fur Y, Décorps M (1994) In vivo, ex vivo, and in vitro one- and two-dimensional nuclear magnetic resonance spectroscopy of an intracerebral glioma in rat brain: assignment of resonances. J Neurochem 62(1):166–179
20. Keilhoff G, Wolf G (1993) Comparison of double fluorescence staining and LDH-test for monitoring cell viability in vitro. Neuroreport 5:129–132
21. Suber L, Foglia S, Romero H, Montone A, Roig A, Casas Ll, Molins E, Fiorani D (2004) Synthesis, morphological-structural characterization and magnetic properties of amorphous iron(III)-oxyhydroxy-phosphate nanoparticles. J Solid State Chem Soc 177:2439–2447
22. Rodríguez E, Gich M, Roig A, Molins E, Nedelko N, Slawska-Waniewska A, Szewczyk A (2006) Investigations of the stability of $\{[(tacn)_6Fe_8(\mu_3\text{-}O)_2(\mu_2\text{-}OH)_{12}]Br_7(H_2O)\}Br \cdot 8H_2O$ (Fe8) cluster in aqueous solution by spectroscopic and magnetic methods. Polyhedron 25:113–118
23. Cha S, Johnson G, Wadghiri YZ, Jin O, Babb J, Zagzag D, Turnbull DH (2003) Dynamic, contrast-enhanced perfusion MRI in mouse gliomas: correlation with histopathology. Magn Reson Med 49(5):848–855
24. Meyer MH, Dulde E, Meyer RA (2004) The genomic response of the mouse kidney to low-phosphate diet is altered in X-linked hypophosphatemia. Physiol Genomics 18:4–11
25. Zoula S, Herigault G, Ziegler A, Farion R, Décorps M, Rémy C (2003) Correlation between the occurrence of 1H-MRS lipid signal, necrosis and lipid droplets during C6 rat glioma development. NMR Biomed 16(4):199–212
26. Locatelli F, Rossi F (2005) Incidence and pathogenesis of tumor lysis syndrome. Contrib Nephrol 147:61–68
27. Mansour AN, Thompson C, Theil EC, Chasteen ND, Sayers DE (1985) Fe(III)·ATP complexes. Models for ferritin and other polynuclear iron complexes with phosphates. JBC 13:7975–7979
28. Zhang Z, van den Bos EJ, Wielopolski PA, de Jong-Popijus M, Duncker DJ, Krestin GP (2004) High-resolution magnetic resonance imaging of iron-labeled myoblasts using a standard 1.5-T clinical scanner. Magn Reson Mater Phy 17: 201–209
29. Walczak P, Kedziorek DA, Gilad AA, Lin S, Bulte JW (2005) Instant MR labeling of stem cells using magnetoelectroporation. Magn Reson Med 54:769–774